Magnetic order in a Cu^{II}-Dy^{III} oxamato-based two-dimensional coordination polymer

ALEJANDRO PASCUAL-ÁLVAREZ,[1] JOAN CANO,*[,1] FRANCESC LLORET,[1] JESÚS FERRANDO-SORIA,[1] DONATELLA ARMENTANO[2] AND EMILIO PARDO*[,1]

[1]Departament de Química Inorgànica, Instituto de Ciencia Molecular (ICMOL), Universitat de València, 46980 Paterna, València, Spain

[2]Dipartimento di Chimica e Tecnologie Chimiche, Università della Calabria, Rende 87036, Cosenza, Italy

e–mail: joan.cano@uv.es; emilio.pardo@uv.es

Abstract

We report the synthesis, crystal structure and magnetic characterization of a novel two-dimensional copper(II)-dysprosium(III) coordination polymer of formula $[Li^{I}(OH_2)_4]_2[Dy^{III}Cu^{II}_2(Me_2pma)_4Cl(H_2O)] \cdot 4H_2O$ (**1**) [Me_2pma = N-2,6-dimethylphenyloxamate]. Compound **1** was obtained by using the mononuclear anionic complex, $[Cu^{II}(Me_2pma)_2]^{2-}$, as a bis(bidentate) metalloligand toward solvated dysprosium(III) cations and shows a square $[Dy^{III}Cu^{II}_2]$ layered structure of $(4^4.6^2)$ net topology. Interestingly, the combination of two factors, the well-known efficiency of oxamato ligands to transmit strong magnetic couplings between neighboring atoms and such structural topology, is responsible for the observation of a ferromagnetic interaction between copper(II) and dysprosium(III) cations and a magnetic ordering (T_C = 7.5 K), paving the way for the obtention of novel future examples of the still very scarce magnetically ordered lanthanide-based coordination polymers.

Keywords

Coordination polymer, magnetic properties, dysprosium, copper

1. Introduction

The possibility to combine, in a single material, interesting physical properties[1] with thrilling architectures,[2] make extended coordination polymers (CPs)[1,3–5] very attractive compounds for scientists working in the multidisciplinary field of coordination chemistry. In particular, the myriad of intriguing magnetic properties that CPs can present are particularly appealing to design materials of interest in the field of molecular magnetism.[6,7] They can include such varied properties as slow magnetic relaxation effects,[8] when single-ion magnets (SIMs)[9–14] constitute the nodes of the network and, more commonly, the appearance of a spontaneous magnetization below a critical temperature (T_C).[15]

In connection with the last point, a careful choice of paramagnetic ions and organic ligands, capable to transmit the magnetic coupling in the appropriate way, turns out to be crucial

in designing CPs exhibiting a long-range magnetic ordering. In addition, an accurate control of the coordination network structure, which is not easy as a consequence of the many subtle factors that may affect the assembly process,[16,17] should be achieved. For example, oxamato-ligands[18] have already shown to be effective in two ways: Firstly, transmitting, efficiently, the magnetic coupling (ferro-[19–21] or antiferromagnetic[22,23]) between neighboring metal atoms. Secondly, allowing the rational synthesis of two- (2D)[24–26] and three-dimensional (3D)[27–34] magnets with first row transition metals through their free carbonyl groups (Scheme S1). Therefore, they seem to be a good choice for the design of new magnets. About paramagnetic metal ions, most examples with oxamato ligands reported so far, involve only 3d metal ions.[35] In this context, it is rather paradoxical the lack of examples of CPs with lanthanide(III) ions exhibiting a long-range magnetic ordering, taking into account that rare-earth garnets**,** alloys and oxides usually exhibit magnetic order and they effectively find application in industry.[36] This is usually explained considering that lanthanide(III) ions (where unpaired electrons are in inner 4f orbitals) exhibit very weak magnetic couplings.[37] The most common strategy to overcome this situation relies on the use of radicals[38–40] or ligands (such as CN^-)[41–47] capable to allow very strong magnetic couplings, and thus, long-range magnetic ordering. In any case, it is clear that novel examples of lanthanide-based compounds with organic ligands showing strong magnetic interactions are still interesting.

Overall, even if many lanthanide-based SIMs,[48] Single-Molecule (SMMs)[49] and Single-Chain Magnets (SCMs)[50] have been reported, as said above, examples of high-dimensional lanthanide-based magnets are still very scarce and much work remains to be done. Olivier Kahn and others explored the efficiency oxamato and oxamidato ligands to transmit the magnetic coupling between 3d and 4f metal ions. So, he published a few pioneering works reporting 3d-4f 1D and 2D Cu^{2+}-Ln^{3+} CPs[51] showing infinite chains,[52] ladder-like type[53,54] and honeycomb[55] architectures, respectively, these compounds, with the only

exception of the very poorly diffracting $Nd_2[Cu(opba)_{0.5}(ox)]_3(DMF)_9$,[51] lacked of X-ray characterization and long-range ferromagnetic orderings could be observed only at such low temperature as 1.78 K.[55]

2. Results and discussion

In this work, we use the "complex-as-ligand" approach[56] for the rational synthesis of a novel 3d-4f CP. We have previously demonstrated[35] that a variety of oxamato-based copper(II) precursor complexes can be used as building blocks, through their free carbonyl oxygen atoms of their oxamate groups, for the rational synthesis of high-dimensional CPs. In particular, taking as a basis Kahn's work and our results with the anionic oxamato-based mononuclear copper(II) complex, $[Cu^{II}(Me_2pma)_2]^{2-}$ (Scheme S1) [Me_2pma = N-2,6-dimethylphenyloxamate],[25,57] which already led to successful results with transition metal ions. Herein we report and characterize structurally, a new 2D CP, of formula $[Li^{I}(OH_2)_4]_2[Dy^{III}Cu^{II}_2(Me_2pma)_4ClH_2O]$ (**1**) showing a ferromagnetic interaction through the oxamato bridges connecting the copper(II) and dysprosium(III) centers. The crystal structure could be resolved allowing a relationship between the structure and the magnetic properties of **1**.

Cubic prisms of **1**, suitable for X-ray diffraction, were obtained after some days of slow evaporation of a water/acetonitrile/methanol solution (1:10:10 volume ratio) containing stoichiometric amounts of $Li_2[Cu^{II}(Me_2pma)_2] \cdot 2H_2O$ and $DyCl_3$ with an excess of LiCl (see Supporting Information). Interestingly, the excess of LiCl seems to play a key role in the crystallization process that leads to the formation of the final network. This behavior can be attributable to different parameters like solubility, supramolecular interactions such as hydrogen bonds (see structural section), ionic force and/or equilibrium displacement.

2.1 Crystal Structure

Compound **1** crystallizes in the *I4/m* space group of the tetragonal system (Table S1, Supporting Information). The structure of **1** consists of an anionic 2D network, $\{Dy^{III}[Cu(Me_2pma)_2]_2Cl(H_2O)\}^{2-}$, and $Li(H_2O)_4^+$ countercations, which are intercalated within adjacent square-grid layers of $(4^4 \cdot 6^2)$ net topology growing in the *ab* plane (Fig. S1), together with disordered crystallization water molecules (Fig. 1).

Within the anionic oxamato-bridged framework of **1**, each Cu^{II} ion is surrounded by two Dy^{III} ions while each Dy^{III} ion is surrounded by four Cu^{II} ions, accounting thus for the final 2:1 Cu:Dy stoichiometry (Figs. 1a-b). So that, each square-grid is defined by Dy^{III} corners and Cu^{II} ions residing in the middle of the square-side arranged pretty close to an ideal square grid with a Cu(1)-Dy(1)-Cu(1c) [(c) = *y*, -*x*, *z*] angle of 88.7°. Furthermore, squares are decorated and almost entirely filled by the aromatic rings of the oxamate ligands pointing inward the pores.

Overall, the connectivity of the Cu^{II} and Dy^{III} ions in **1**, acting as bi- and tetra-connectors (Fig. S2), respectively, yield 2D net similar to those found when reacted *n*-Bu_4N salt of the copper(II) precursor $[Cu^{II}(Me_2pma)]^{2-}$ and the nitrate salt of the Sr^{II} and Ba^{II} ions (Figs. 1c-b).[58] Each Cu^{II} ion is tetra-coordinated by two bis(bidentate) oxamate bridging ligands in a square-planar CuN_2O_2 geometry [with average Cu–O and Cu-N bond distances of 1.86(2) and 1.85(5) Å, respectively]. In turn, the Dy^{III} ions are ten-coordinated being surrounded by four oxamate bridges from different $[Cu^{II}(Me_2pma)]^{2-}$ entities, a chlorine and a water molecule in a distorted bicapped cubic geometry MnO_9Cl (Fig. 2). The two crystallographically distinct Dy-$O_{oxamate}$ bond lengths of 2.37(1) and 2.44(2) Å [for Dy-O2 and Dy-O3 and their symmetrically equivalents, respectively (Fig. 2a)], are shorter than the Dy-O_w [2.59(2) Å for Dy-O4] and Dy-Cl [2.62(3) Å] ones but in agreement with those found in literature for analogue environments.[59,60]

Eclipsed anionic heterobimetallic open-frameworks of **1** (Figs. S3 and S4) interact with $Li(H_2O)_4^+$ cations through multiple hydrogen-bonding O(oxamate)···H-Ow host-guest

interactions [O(oxamate)···H-Ow of 3.02(4) Å] (Figs. 1, 3, S2 and S4) describing a supramolecular motif reminiscent of Li-ion batteries where solvated alkali metals ions are intercalated within anionic graphite-like layers. As shown in Fig. 3, hydrophobic and hydrophilic regions alternate, as result of the disposition of the dimethyl-substituted phenylene spacers, pointing outwards or inwards of the voids, respectively. The terminal chlorine atoms are pretty confined in the hydrophilic sides, being the aforementioned Li^+ intercalation further stabilized or likely driven by hydrogen bonds involving $Li(H_2O)_4^+$ cations and the coordinated water molecules [Li-Ow···H-O1w of 2.9(4) Å].

Even if it was not possible to find a reasonable model for the disordered water molecules (see Supporting Information), the structural analysis revealed an estimated volumes of accessible solvent voids of 1936.1 $Å^3$ that represent up to 29.7% of the total unit cell volume [6190.5 $Å^3$]. This feature would likely account for the embedding co-crystallized water molecules placed within the sheets, in good agreement with the elemental analyses for **1**.

2.2 Thermogravimetric Analysis and X-Ray Powder Diffraction of 1

The solvent contents of compound **1** were determined by thermogravimetric analysis (TGA) under dry N_2 (Fig. S5). It shows a very fast mass loss from room temperature to around 70 °C, followed by a *plateau* under further heating up to 200 °C, when decomposition starts. Overall, the mass loss of *ca.* 18.5% at 150 °C corresponds to *ca.* 13 molecules per formula unit, and, together with CHN analyses, determine the final chemical nature of the compound (see Supporting Information).

Powder X-ray diffraction (PXRD) pattern, carried out on a polycrystalline sample of **1** (Fig. 4), confirms the isostructurality with the crystal selected for single crystal X-ray diffraction and pureness of the bulk.

2.3 Magnetic properties

Fig. 5a shows the temperature dependence of the direct current (dc) magnetic susceptibility of **1**, in the form of the $\chi_M T$ versus T plot (χ_M being the dc molar magnetic susceptibility per Cu_2Dy unit). At room temperature (R. T.), $\chi_M T$ value for **1** (14.76 cm^3 K mol^{-1}), is similar to that expected for the sum of two square planar Cu^{II} ions ($\chi_M T$ = 0.80 cm^3 mol^{-1} K with g_{Cu} = 2.1 and S_{Cu} = ½) and one Dy^{III} ion [$\chi_M T = (N\beta^2 g_{Dy}^2/3k_B)J(J+1)$ = 14.15 cm^3 mol^{-1} K with J =15/2 and g_{Dy} = 4/3]. Upon cooling, $\chi_M T$ for **1** decreases, most-likely as a consequence of the first-order angular momentum and crystal field effects of the Dy^{III} ion[61] ($^6H_{15/2}$ term with S = 5/2 and L = 5), and it attains a minimum at *ca.* 14 K (inset of Fig. 5a). Below the minimum, $\chi_M T$ increases sharply to reach a $\chi_M T$ = 19.32 cm^3 K mol^{-1} value at 2.0 K. Such a sharp increase below 14 K (Fig. 5a) can hardly be explained only through intra-layer ferromagnetic interactions. Antiferromagnetic interactions between Cu^{II} and Dy^{III} ions could turn **1** into a ferrimagnetic system with also a sharp increase of $\chi_M T$ at low temperatures. However, the observed minimum value of $\chi_M T$ is too high, exceeding that expected for two Cu^{II} ions magnetically uncoupled to the ground doublet of the Dy^{III} ion.

The *M versus H* plots (*M* being the molar magnetization per Cu_2Dy unit and *H* the applied *dc* magnetic field) at 2.0 K (Fig. 5b) further confirm this ferromagnetic behavior. The isothermal magnetization curve of **1** exhibits a quite fast saturation with a maximum *M* value of 6.55 $N\beta$ at 5.0 T, which is very similar to that expected considering a parallel alignment of the spins of two Cu^{II} (S_{Cu} = 1/2) and one Dy^{III} (S_{Dy} = 5/2) ions, thus suggesting a particularly strong ferromagnetic interaction between neighboring metal ions. However, no hysteresis was observed for this compound at 2.0 K because of its small value, requiring a lower temperature to allow its record. To these experimental features, it should add that within the 2D anionic $Cu^{II}_2Dy^{III}$ and 1D neutral $Cu^{II}Dy^{III}$ networks, the ferromagnetic nature of the magnetic coupling between the Dy^{III} and the Cu^{II} ions through the oxamate bridge was already reported in the past.[54,62] Therefore, it seems obvious to expect that the observed magnetic behavior is a

consequence of a ferromagnetic intra-layer coupling. So, even if $\chi_M T$ decreases in the range 300-14 K for **1**, due to the depopulation of the excited Stark sublevels of Dy^{III} ions, the ferromagnetic interaction within the plane can slightly mask this drop of $\chi_M T$.

Unfortunately, there is no analytical expression capable of simulating the magnetic behavior of this regular 2D network, but containing two different metal ions and one of them with coupled spin and angular momenta. This last point makes particularly tricky the study of the magnetic properties, even more, when some effects are acting at the same time, that is, when the effect of the magnetic coupling is playing its role during the depopulation of the excited doublets caused by the SOC on the Dy^{III} ion. In other words, some methodologies based on effective unities could help in a relatively simple way when a phenomenon is dominant; but in **1** the magnetic coupling is strong enough to its effect comes together with those from SOC shown by the Dy^{III} ion. In such circumstances, the simulation of the magnetic behavior of **1** becomes an impossible task.

So, the experimental data above 50 K, where the influence of the magnetic coupling is not significant yet, was analyzed. The spin Hamiltonian used and summarized in Eq. (1) embodies the SOC of the Dy^{III} ion, and the Zeeman effect of this ion and two uncoupled Cu^{II} ions. Structural distortions in the coordination sphere of the Dy^{III} ion appear as an axial zfs parameter (Δ) on its angular momentum. The spin-orbit coupling constant was considered constant and equal to the value of the free ion (λ = –380 cm^{-1}). The ideal spin momentum (S = 5/2) for the Dy^{III} ion in this model has, therefore, a g-factor equal to 2.0, the value for the free electron (g_e). The low delocalization of the *f* orbitals in the rare earth complexes supports the assignation of the unity as value for κ. Having in mind these particularities, with a g-factor of 2.00 for the Cu^{II} ion (g_{Cu}), the Δ parameter for the best-fit above 50 K takes a value of +66.5 cm^{-1}, which is in agreement with values for other dysprosium(III) complexes reported previously.[54] The agreement factor between experimental and simulated data, and defined as

$F = \sum\left(P_{exp} - P_{calcd}\right)^2 / \sum P_{exp}^2$ being P the measured physical property, is F = 1.6 x 10^{-5}. A simulation with these values agrees reasonably well with the experimental curve; however, it is not perfect even removing any restraint on the values of λ and κ. Probably, a possible effect of the magnetic coupling occurs even above 50 K, which, if small or moderate, was also observed in a Dy_2Cu_3 network with oxamate as bridging ligand.[54]

$$\hat{H} = \lambda \hat{L}\hat{S} + \Delta\left[\hat{L}_z^2 - L\,(L+1)/3\right] + \beta H\left(g_e \hat{S} - k\hat{L} + g_{Cu}\hat{S}_{Cu}\right) \qquad (1)$$

CASSCF/NEVPT2 calculations on a $DyCu_4$, or even on a DyCu model, could procure both the splitting of the ground term promoted of the ligand field on the Dy^{III} ion and the magnetic coupling between Dy^{III} and Cu^{II} ions. This study is prohibitively expensive because of the excessive size of the chosen active space to build the ground and excited states. Besides, the magnetic interaction between 4*f* and 3*d* ions involve the empty 5*d* orbitals of the lanthanoid ions, which requires an enormous increase of the active space.[63–65] Moreover, these factors make difficult the convergence of this kind of calculations. Since there can be no doubt about the ferromagnetic nature between Dy^{III} and Cu^{II} ions, choosing a model that allows studying only the splitting of the f orbitals and the ground term promoted of the ligand field on the Dy^{III} ion is a good option. In this case, from the experimental geometry of **1**, the appropriate model ($DyZn_4$) is built replacing paramagnetic Cu^{II} ions by diamagnetic Zn^{II} ones in, keeping the electronic features of the chemical surrounding (Fig. 6). This splitting leads to a few low-lying excited sextets very near to the ground state (Figs. 7 and S6), such as demonstrated the CASSCF/NEVPT2 calculations. Specifically, ten of these excited states are in the range of 1161 cm^{-1}, and three of them place only 31, 258 and 266 cm^{-1} above the ground state. This fact agrees with a stronger influence of the SOC on the splitting of the states and the magnetic properties than the ligand-field effect. By the previous discussion about the analysis of the

magnetic data, the presence of close low-lying excited states makes difficult the analysis of the simulation of the magnetic behavior of **1**, which becomes impossible when the magnetic couplings throughout the 2D network are included. Next sextet excited states are placed over 7550 cm^{-1} above the ground state. Quartet excited states are beyond 24000 cm^{-1}.

On the other hand, ten donor atoms organized in a bicapped square prism constitute the coordination sphere of the Dy^{III} ion. In this coordination polyhedron, four chelating oxamate ligands in "equatorial" positions occupy the eight vertices of the square prism. Considering each oxamate ligand with two coordinate donor atoms as an only coordination point, the coordination would look like an octahedron in a D_{4h} symmetry and with four oxamate ligands in its equatorial plane, being this the cause of the use of "equatorial" term in the present discussion. Whereas the Dy-O(oxamate) bond lengths are longer than in a previous system, The Dy-O(water) is shorter than the majority of the reported dysprosium(III) compounds. The weaker ligand-field of "axially" coordinate chloride and water ligands than the "equatorial" oxamate groups makes the dysprosium(III) compound shows an in-plane anisotropy.[66–68] That is, an easy-magnetization appears in the "equatorial" plane, which divides the coordination polyhedron into two separate square pyramids. This particular magnetic anisotropy could spread throughout the 2D $DyCu_2$ network through intra-layer ferromagnetic couplings.

Compound **1** shows a paramagnetic-to-ferromagnetic phase transition at T_C = 7.5 K, which is confirmed by both (*i*) the presence of sharp non-frequency-dependent peaks at 7.5 K in the χ''_M *vs. T* plot (Fig. 8a) and (*ii*) the divergence of the field-cooled magnetization (FCM) and the zero-field-cooled magnetization (ZFCM) curves at the same temperature (Fig. 8b). In general, a 2D network cannot display a magnetic order, but **1** does. The non-frequency dependent of the χ''_M peaks (Fig. 8) rules out a slow relaxation of the magnetization on the Dy^{III} ion. On the other hand, the presence of moderate ferromagnetic intra-layer interaction cannot explain this magnetic ordering without the inclusion of (*i*) ferromagnetic inter-layer

interaction between neighboring planes, or (*ii*) a magnetic anisotropy, that is, that **1** behaves as a magnetic XY plane.[69] The first case is based on the most-likely dipolar nature of the interactions, but they are often weak and antiferromagnetic. However, in **1**, the first-order SOC in the Dy^{III} ion with an in-plane anisotropy transfers a magnetic anisotropy to the $DyCu_2$ layer, being this an XY plane where a long-range magnetic ordering is possible without the presence of the interlayer couplings, which seems reasonable from the crystal structure. Yet the behavior of this kind of 2D systems is not simple. They exhibit a particular phase transition of infinite order from high-temperature disorder phase to a low-temperature quasi ordered phase. However, they can explain the observed behavior for **1**. Interestingly, although a good number of oxamato-based CPs merely with 3d metal ions and exhibiting ferromagnetic ordering have been reported, ferromagnetic ordering in CPs involving 4*f* metals are very rare. Thus, with isolated exceptions, such as, polymeric compounds involving interchain interactions[40,45] and a 2D compound reported by Kahn, in which a ferromagnetic ordering was observed below 2.0 K by specific heat measurements,[55] compound **1** is one of the very first 3*d*-4*f* magnets and indeed exhibits the largest T_C reported so far for lanthanide-based CPs.

3. Conclusions

In conclusion, we report a novel two-dimensional (2D) oxamato-based copper(II)-dysprosium(III) coordination polymer (CP), which was obtained following a rational programmed strategy. The 2D CP shows a square $[Dy^{III}Cu^{II}_2]$ layered structure of $(4^4 \cdot 6^2)$ net topology. Interestingly, the combination of two factors, the well-known efficiency of oxamato ligands to transmit strong magnetic couplings between neighboring atoms and the mentioned structural topology, is responsible for the observation of ferromagnetic interactions between copper(II) and dysprosium(III) cations, allowing the presence of a ferromagnetic ordering, very

uncommon in lanthanide-based CPs. Current efforts are devoted to study the influence of the hydration/dehydration processes in the magnetic properties.

4. Experimental section

4.1 Materials

All chemicals were of reagent grade quality. They were purchased from commercial sources and used as received. The proligand HEt-Me_2pma and the mononuclear copper(II) complex (*n*-$Bu_4N)_2[Cu(Me_2pma)_2] \cdot 2H_2O$ were prepared as previously reported.[25,57] Preparation of $Li_2[Cu(Me_2pma)_2] \cdot 2H_2O$ is given in detail in the Supporting Information.

4.2 Preparation of $[Li^I(OH_2)_4]_2[Dy^{III}Cu^{II}_2(Me_2pma)_4ClH_2O] \cdot 4H_2O$ (1)

Well-formed dark green prisms of **1**, which were suitable for X-ray diffraction, were obtained by slow evaporation of 10 mL of a water/acetonitrile/methanol solution (1:10:10 volume ratio) containing stoichiometric amounts of $Li_2[Cu^{II}(Me_2pma)_2] \cdot 2H_2O$ (0.10 g, 0.20 mmol) and $DyCl_3$ (0.027 g, 0.10 mmol) with an excess of LiCl (0.5 mmol). After several days standing on air, green crystals of **1** appeared. They were filtered off and air-dried. Yield: 59%; Elemental analysis calcd. (%) for $C_{40}H_{62}Cu_2DyLi_2N_4O_{25}Cl$ (1337.9): C 35.91, H 4.67, N 4.18; found: C 35.78, H 4.59, N 4.21; IR (KBr): ν = 1601 (C=O).

4.3 Single-Crystal X-ray Diffraction

Crystal data for **1**: $C_{40}H_{652}Cu_2DyLi_2N_4O_{21}Cl$, M_r = 1236.76, tetragonal, space group *I*4/*m*, a = 15.9307(5), c = 24.3926(9) Å, V = 6190.5(5) Å^3, T = 90(2) K, λ = 0.71073Å, Z = 4, ρ_{calc} = 1.356 g cm^{-3}, μ = 1.983 mm^{-1}, 2188 unique reflections [35182 measured (R_{int} = 0.0270)] and 1898 observed with $I > 2\sigma(I)$, 1.53º ≤ θ ≤ 25.24º, R = 0.1319 (0.1380 for all data), wR = 0.3715 (0.3806 for all data) with 114 parameters and 18 restraints, the final Fourier-difference map showed maximum and minimum height peaks of 4.144 and -3.600 e Å^{-3}. Crystal structure deposited at Cambridge Crystallographic Database with CCDC 1891550.

Single crystal of **1** was mounted on glass fibers, in a grease drop and very quickly placed on a liquid nitrogen stream cooled at 100 K to avoid the degradation upon dehydration. Diffraction data were collected on a Bruker-Nonius X8APEXII CCD area detector diffractometer using graphite-monochromated Mo-K_α radiation (λ = 0.71073 Å). The data were processed through the SAINT[70] reduction and SADABS[71] multi-scan absorption software. Despite the high quality of the full set of data with a quite low θ_{max} of diffraction (θ = 27°) were obtained (detected as Alerts A in the checkcif), even if many efforts have been made to extract the best diffraction data from sample. Furthermore, high residual electron density which are at less than 1 Å from the metal atom, are due to the effect of the dysprosium and even copper ripples. However, the solution and refinement parameters are suitable, compared with analogue MOFs structures previously reported, thus we are convinced that the structure found is consistent.[72–75]

The structure was solved by the Patterson method and subsequently completed by Fourier recycling using the SHELXL-2013 software package.[76,77] All non-hydrogen atoms were refined anisotropically except Li^+ alkali metal and some disordered carbon or oxygen atoms from ligands and water molecules. The hydrogen atoms were set in calculated positions and refined as riding atoms. The high thermal vibration parameters (Alerts A and B in the checkcifs) displayed for some atoms in the organic ligand are consequence of contributions from different factors, including (a) the flexibility of the framework and consequential disorder, (b) the high residual electron density produced by the methyl groups that are dynamic components of the walls, (c) the use of some bond length and angle restrains during the refinements or fixed positions of some highly disordered atoms. Furthermore, and as expected for such systems, the lattice water molecules were highly disordered and cannot be satisfactory modeled (at the origin of the first levels Alerts A). Those found from ΔF map, were the coordinated ones refined with restraints and their hydrogen atoms were neither found nor

calculated. As a consequence, the contribution to the diffraction pattern from the highly disordered water molecules of crystallization (6 molecules of H_2O located in the voids of the lattice that amount to ca. 30 % percentage void volume of the unit cell), were subtracted from the observed data through the SQUEEZE method, implemented in PLATON.[78] The final formulation for each compound is in consistent with the residual electron density and volume. The final full-matrix least-squares refinements on F^2, minimizing the function $\sum w(|F_o|-|F_c|)^2$, reached convergence with the values of the discrepancy indices given in Table S1. High R values (levels Alert A in checkcifs) are, most likely, mainly affected by the ripples and by contribution of the highly disordered solvent to the intensities of the low angle reflections. The final geometrical calculations and all the graphical aspects were carried out with CRYSTAL MAKER, and WinGX.[79–81]

4.4 X-ray Powder Diffraction

A Polycrystalline sample of **1** was introduced into a 0.5 mm borosilicate capillary and then it was mounted and aligned on a Empyrean PANalytical powder diffractometer, equipped with a CuKα radiation (λ = 1.54056 Å). For each sample, five measurements were collected at room temperature (2θ = 2–40°) and merged in a single diffractogram.

4.5 X-ray Powder Diffraction

A Polycrystalline sample of **1** was introduced into a 0.5 mm borosilicate capillary and then it was mounted and aligned on aN Empyrean PANalytical powder diffractometer, equipped with a CuKα radiation (λ = 1.54056 Å). For each sample, five measurements were collected at room temperature (2θ = 2–40°) and merged in a single diffractogram.

4.6 Magnetic Measurements

Variable-temperature direct current (dc) and alternating current (ac) magnetic susceptibility measurements were carried out with a Quantum Design SQUID magnetometer.

The susceptibility data were corrected for the diamagnetism of both the constituent atoms and the sample holder.

4.7 Theoretical calculations

In order to evaluate the splitting of the states promoted by crystal-field on the Dy^{III} ion in **1**, the relative energies of the ground and low-lying excited states were computed by calculations based on the second order N–electron valence state perturbation theory (NEVPT2) applied on the wave function, which was previously obtained from complete active space (CAS) calculation. These calculations were performed with the version 4.0 of the ORCA programme on a $DyZn_4$ molecular model built from the experimental geometry of **1** and by replacing paramagnetic Cu^{II} ions by diamagnetic Zn^{II} ones, in order to keep to the utmost, the electronic features of the system.[82] The TZVP basis set proposed by Ahlrichs and the auxiliary TVZ/C Coulomb fitting basis sets were used for all atoms.[83,84] Electronic relativistic effects introduced by the dysprosium atom were considered through the ZORA Hamiltonian[85] and the SARC (segmented all-electron relativistically contracted) version of the TZVP basis set (SARC-ZORA-TZVP).[86–90] The energies of 21 sextet and 12 quartet states generated from an active space with nine electrons in seven f orbitals were calculated. See Supporting Information for further details.

Acknowledgement

This work was supported by the MINECO (Spain) (Projects CTQ2016-75671-P and CTQ2016-75068-P) and the Ministero dell'Istruzione, dell'Università e della Ricerca (Italy). A. P.-A. thanks the MINECO for a predoctoral contract. Thanks are also extended to the "Subprograma Atracció de Talent-Contractes Post-doctorals de la Universitat de Valencia" and the "2018 Leonardo Grant for Researchers and Cultural Creators, BBVA Foundation" (J.F.S.). E.P. acknowledges the financial support of the European Research Council under the European

Union's Horizon 2020 research and innova-tion programme / ERC Grant Agreement No 814804, MOF-reactors.

References

[1] C. Janiak, Engineering coordination polymers towards applications, Dalt. Trans. (2003) 2781–2804. doi:10.1039/b305705b.

[2] D. Bradshaw, J.B. Claridge, E.J. Cussen, T.J. Prior, M.J. Rosseinsky, Design, Chirality, and Flexibility in Nanoporous Molecule-Based Materials, Acc. Chem. Res. 38 (2005) 273–282. doi:10.1021/ar0401606.

[3] B.F. Abrahams, B.F. Hoskins, D.M. Michail, R. Robson, Assembly of porphyrin building blocks into network structures with large channels, Nature. 369 (1994) 727–729. doi:10.1038/369727a0.

[4] S.R. Batten, R. Robson, Interpenetrating Nets: Ordered, Periodic Entanglement, Angew. Chem. Int. Ed. 37 (1998) 1460–1494. doi:10.1002/(SICI)1521-3773(19980619)37:11<1460::AID-ANIE1460>3.0.CO;2-Z.

[5] S. Kitagawa, R. Matsuda, Chemistry of coordination space of porous coordination polymers, Coord. Chem. Rev. 251 (2007) 2490–2509. doi:10.1016/j.ccr.2007.07.009.

[6] O. Kahn, Molecular Magnetism, VCH Publishers: New York, 1993.

[7] J. Ferrando-Soria, J. Vallejo, M. Castellano, J. Martínez-Lillo, E. Pardo, J. Cano, I. Castro, F. Lloret, R. Ruiz-García, M. Julve, J. Martinez-Lillo, E. Pardo, J. Cano, I. Castro, F. Lloret, R. Ruiz-Garcia, M. Julve, Molecular magnetism, quo vadis? A historical perspective from a coordination chemist viewpoint, Coord. Chem. Rev. 339 (2017) 17–103. doi:10.1016/j.ccr.2017.03.004.

[8] J. Gatteschi, D; Sessoli, R.; Villain, Molecular Nanomagnets, Oxford University Press, 2006.

[9] X. Liu, L. Sun, H. Zhou, P. Cen, X. Jin, G. Xie, S. Chen, Q. Hu, Single-Ion-Magnet Behavior in a Two-Dimensional Coordination Polymer Constructed from Co II Nodes and a Pyridylhydrazone Derivative, Inorg. Chem. 54 (2015) 8884–8886. doi:10.1021/acs.inorgchem.5b01651.

[10] J. Palion-Gazda, T. Klemens, B. Machura, J. Vallejo, F. Lloret, M. Julve, Single ion magnet behaviour in a two-dimensional network of dicyanamide-bridged cobalt(II) ions, Dalt. Trans. 44 (2015) 2989–2992. doi:10.1039/C4DT03574G.

[11] A.E. Ion, S. Nica, A.M. Madalan, S. Shova, J. Vallejo, M. Julve, F. Lloret, M. Andruh, Two-Dimensional Coordination Polymers Constructed Using, Simultaneously, Linear and Angular Spacers and Cobalt(II) Nodes. New Examples of Networks of Single-Ion Magnets, Inorg. Chem. 54 (2015) 16–18. doi:10.1021/ic5025197.

[12] J. Vallejo, F.R. Fortea-Pérez, E. Pardo, S. Benmansour, I. Castro, J. Krzystek, D. Armentano, J. Cano, Guest-dependent single-ion magnet behaviour in a cobalt(II) metal–organic framework, Chem. Sci. 7 (2016) 2286–2293. doi:10.1039/C5SC04461H.

[13] G. Brunet, D.A. Safin, J. Jover, E. Ruiz, M. Murugesu, Single-molecule magnetism arising from cobalt(II) nodes of a crystalline sponge, J. Mater. Chem. C. 5 (2017) 835–841. doi:10.1039/C6TC04703C.

[14] C. Qiao, L. Sun, S. Zhang, P. Liu, L. Chang, C.-S. Zhou, Q. Wei, S. Chen, S. Gao, Pore-size-tuned host–guest interactions in Co-MOFs via in situ microcalorimetry: adsorption and magnetism, J. Mater. Chem. C. 5 (2017) 1064–1073. doi:10.1039/C6TC05082D.

[15] M.M. Turnbull, T. Sugimoto, L.K. Thompson, eds., Molecule-Based Magnetic Materials, American Chemical Society, Washington, DC, 1996. doi:10.1021/bk-1996-0644.

[16] M.G. Goesten, F. Kapteijn, J. Gascon, Fascinating chemistry or frustrating unpredictability: observations in crystal engineering of metal–organic frameworks, CrystEngComm. 15 (2013) 9249–9257. doi:10.1039/c3ce41241e.

[17] F.M. Tabellion, S.R. Seidel, A.M. Arif, P.J. Stang, Discrete Supramolecular Architecture vs Crystal Engineering: The Rational Design of a Platinum-Based Bimetallic Assembly with a Chairlike Structure and Its Infinite, Copper Analogue, J. Am. Chem. Soc. 123 (2001) 7740–7741. doi:10.1021/ja015784a.

[18] T. Grancha, J. Ferrando-Soria, M. Castellano, M. Julve, J. Pasán, D. Armentano, E. Pardo, Oxamato-based coordination polymers: recent advances in multifunctional magnetic materials., Chem. Commun.. 50 (2014) 7569–7585. doi:10.1039/c4cc01734j.

[19] E. Pardo, D. Cangussu, M.-C. Dul, R. Lescouëzec, P. Herson, Y. Journaux, E.F. Pedroso, C.L.M. Pereira, M.C. Muñoz, R. Ruiz-García, J. Cano, P. Amorós, M. Julve, F. Lloret, A metallacryptand-based manganese(II)-cobalt(II) ferrimagnet with a three-dimensional honeycomb open-framework architecture., Angew. Chem. Int. Ed. Engl. 47 (2008) 4211–6. doi:10.1002/anie.200800208.

[20] I. Fernndez, R. Ruiz, J. Faus, M. Julve, F. Lloret, J. Cano, X. Ottenwaelder, Y. Journaux, M. Carmen Muoz, Ferromagnetic coupling through spin polarization in a dinuclear copper(n) metallacyclophane, Angew. Chem. Int. Ed. 40 (2001). doi:10.1002/1521-3773(20010817)40:16<3039::AID-ANIE3039>3.0.CO;2-P.

[21] M.-C.M.-C. Dul, E. Pardo, R. Lescouezec, L.-M.L.-M. Chamoreau, F. Villain, Y. Journaux, R. Ruiz-Garcia, J. Cano, M. Julve, F. Lloret, J. Pasan, C. Ruiz-Perez, R. Lescouëzec, L.-M.L.-M. Chamoreau, F. Villain, Y. Journaux, R. Ruiz-García, J. Cano, M. Julve, F. Lloret, J. Pasán, C. Ruiz-Pérez, Redox Switch-Off of the Ferromagnetic Coupling in a Mixed-Spin Tricobalt(II) Triple Mesocate, J. Am. Chem. Soc. 131 (2009) 14614–14615. doi:10.1021/ja9052202.

[22] E. Pardo, J. Faus, M. Julve, F. Lloret, M.C.C. Muñoz, J. Cano, X. Ottenwaelder, Y. Journaux, R. Carrasco, G. Blay, I. Fernández, R. Ruiz-García, Long-Range Magnetic Coupling through Extended π-Conjugated Aromatic Bridges in Dinuclear Copper(II) Metallacyclophanes, J. Am. Chem. Soc. 125 (2003) 10770–10771. doi:10.1021/ja030060f.

[23] E. Pardo, R. Carrasco, R. Ruiz-García, M. Julve, F. Lloret, M.C. Muñoz, Y. Journaux, E. Ruiz, J. Cano, Structure and Magnetism of Dinuclear Copper(II) Metallacyclophanes with Oligoacenebis(oxamate) Bridging Ligands: Theoretical Predictions on Wirelike Magnetic Coupling, J. Am. Chem. Soc. 130 (2008) 576–585. doi:10.1021/ja0747066.

[24] J. Ferrando-Soria, J. Pasán, C. Ruiz-Pérez, Y. Journaux, M. Julve, F. Lloret, J. Cano, E. Pardo, Spin control in oxamato-based manganese(II)-copper(II) coordination polymers with brick-wall layer architectures., Inorg. Chem. 50 (2011) 8694–6. doi:10.1021/ic201437u.

[25] J. Ferrando-Soria, T. Grancha, M. Julve, J. Cano, F. Lloret, Y. Journaux, J. Pasan, C. Ruiz-Perez, E. Pardo, J. Pasán, C. Ruiz-Pérez, E. Pardo, Ligand effects on the dimensionality of oxamato-bridged mixed-metal open-framework magnets, Chem. Commun. 48 (2012) 3539–3541. doi:10.1039/c2cc17767f.

[26] J. Ferrando-Soria, H. Khajavi, P. Serra-Crespo, J. Gascon, F. Kapteijn, M. Julve, F. Lloret, J. Pasán, C. Ruiz-Pérez, Y. Journaux, E. Pardo, Highly selective chemical sensing in a luminescent nanoporous magnet., Adv. Mater. 24 (2012) 5625–9. doi:10.1002/adma.201201846.

[27] H.O. Stumpf, Y. Pei, O. Kahn, L. Ouahab, D. Grandjean, A Molecular-Based Magnet with a Fully Interlocked Three-Dimensional Structure, Science. 261 (1993) 447–449. doi:10.1126/science.261.5120.447.

[28] J. Ferrando-Soria, P. Serra-Crespo, M. de Lange, J. Gascon, F. Kapteijn, M. Julve, J. Cano, F. Lloret, J. Pasan, C. Ruiz-Perez, Y. Journaux, E. Pardo, Selective Gas and Vapor Sorption and Magnetic Sensing by an Isoreticular Mixed-Metal-Organic Framework, J. Am. Chem. Soc. 134 (2012) 15301–15304. doi:10.1021/ja3045822.

[29] J. Ferrando-Soria, R. Ruiz-García, J. Cano, S.-E. Stiriba, J. Vallejo, I. Castro, M. Julve, F. Lloret, P. Amorós, J. Pasán, C. Ruiz-Pérez, Y. Journaux, E. Pardo, Reversible solvatomagnetic switching in a spongelike manganese(II)-copper(II) 3D open framework with a pillared square/octagonal layer architecture., Chem. Eur. J. 18 (2012) 1608–17. doi:10.1002/chem.201103308.

[30] T. Grancha, J. Ferrando-Soria, H.-C. Zhou, J. Gascon, B. Seoane, J. Pasán, O. Fabelo, M. Julve, E. Pardo, Postsynthetic Improvement of the Physical Properties in a Metal-Organic Framework through a Single Crystal to Single Crystal Transmetallation, Angew. Chem. Int. Ed. 54 (2015) 6521–6525. doi:10.1002/anie.201501691.

[31] T. Grancha, M. Mon, F. Lloret, J. Ferrando-Soria, Y. Journaux, J. Pasán, E. Pardo, Double Interpenetration in a Chiral Three-Dimensional Magnet with a (10,3)-a Structure, Inorg. Chem. 54 (2015) 8890–8892. doi:10.1021/acs.inorgchem.5b01738.

[32] T. Grancha, A. Acosta, J. Cano, J. Ferrando-Soria, B. Seoane, J. Gascon, J. Pasan, D. Armentano, E. Pardo, J. Pasán, D. Armentano, E. Pardo, Cation Exchange in Dynamic 3D Porous Magnets: Improvement of the Physical Properties, Inorg. Chem. 54 (2015) 10834–10840. doi:10.1021/acs.inorgchem.5b01854.

[33] A. Abhervé, T. Grancha, J. Ferrando-Soria, M. Clemente-León, E. Coronado, J.C. Waerenborgh, F. Lloret, E. Pardo, Spin-crossover complex encapsulation within a magnetic metal–organic framework, Chem. Commun. 52 (2016) 7360–7363. doi:10.1039/C6CC03667H.

[34] M. Mon, A. Pascual-Álvarez, T. Grancha, J. Cano, J. Ferrando-Soria, F. Lloret, J. Gascon, J. Pasán, D. Armentano, E. Pardo, Solid-State Molecular Nanomagnet Inclusion into a Magnetic Metal-Organic Framework: Interplay of the Magnetic Properties, Chem. Eur. J. 22 (2016) 539–545. doi:10.1002/chem.201504176.

[35] M.-C. Dul, E. Pardo, R. Lescouezec, Y. Journaux, J. Ferrando-Soria, R. Ruiz-Garcia, J. Cano, M. Julve, F. Lloret, D. Cangussu, C.L.M. Pereira, H.O. Stumpf, J. Pasan, C. Ruiz-Perez, Supramolecular coordination chemistry of aromatic polyoxalamide ligands: A metallosupramolecular approach toward functional magnetic materials, Coord. Chem. Rev. 254 (2010) 2281–2296. doi:10.1016/j.ccr.2010.03.003.

[36] T.G. Goonan, Rare earth elements—End use and recyclability: U.S. Geological Survey Scientific Investigations Report 2011–5094, 2011.

[37] C. Benelli, D. Gatteschi, Magnetism of Lanthanides in Molecular Materials with Transition-Metal Ions and Organic Radicals, Chem. Rev. 102 (2002) 2369–2388. doi:10.1021/cr010303r.

[38] L. Norel, L.-M. Chamoreau, Y. Journaux, O. Oms, G. Chastanet, C. Train, Verdazyl-lanthanide(III) one dimensional compounds: synthesis, structure and magnetic properties, Chem. Commun. (2009) 2381. doi:10.1039/b816910a.

[39] M. Ballesteros-Rivas, H. Zhao, A. Prosvirin, E.W. Reinheimer, R.A. Toscano, J. Valdés-Martínez, K.R. Dunbar, Magnetic Ordering in Self-assembled Materials Consisting of Cerium(III) Ions and the Radical Forms of 2,5-TCNQX 2 (X=Cl, Br), Angew. Chem. Int. Ed. 51 (2012) 5124–5128. doi:10.1002/anie.201107938.

[40] E.M. Fatila, A.C. Maahs, M.B. Mills, M. Rouzières, D. V Soldatov, R. Clérac, K.E. Preuss, Ferromagnetic ordering of –[Sm(<scp>iii</scp>)-radical] $_n$ – coordination polymers, Chem. Commun. 52 (2016) 5414–5417. doi:10.1039/C6CC01548D.

[41] F. Hulliger, M. Landolt, H. Vetsch, Rare-earth ferricyanides and chromicyanides LnT(CN)6·nH2O, J. Solid State Chem. 18 (1976) 283–291. doi:10.1016/0022-4596(76)90107-9.

[42] H.-Z. Kou, S. Gao, X. Jin, Synthesis, Crystal Structure, and Magnetic Properties of Two Cyano-Bridged Bimetallic 4f−3d Arrays with One-Dimensional Chain and Two-Dimensional Brick Wall Molecular Structures, Inorg. Chem. 40 (2001) 6295–6300. doi:10.1021/ic0103042.

[43] S. Gao, G. Su, T. Yi, B.-Q. Ma, Observation of an unusual field-dependent slow magnetic relaxation and two distinct transitions in a family of rare-earth–transition-metal complexes, Phys. Rev. B. 63 (2001) 054431. doi:10.1103/PhysRevB.63.054431.

[44] C. Ge, H.-Z. Kou, Z.-H. Ni, Y.-B. Jiang, L.-F. Zhang, A.-L. Cui, O. Sato, Cyano-bridged One-dimensional Sm III –Fe III Molecule-based Magnet with an Ordering Temperature of 3.4 K, Chem. Lett. 34 (2005) 1280–1281. doi:10.1246/cl.2005.1280.

[45] H. Zhao, N. Lopez, A. Prosvirin, H.T. Chifotides, K.R. Dunbar, Lanthanide–3d cyanometalate chains Ln(III)–M(III) (Ln = Pr, Nd, Sm, Eu, Gd, Tb; M = Fe) with the tridentate ligand 2,4,6-tri(2-pyridyl)-1,3,5-triazine (tptz): evidence of ferromagnetic interactions for the Sm(III)–M(III), Dalt. Trans. (2007) 878–888. doi:10.1039/B616016F.

[46] Y. Guo, G.-F. Xu, C. Wang, T.-T. Cao, J. Tang, Z.-Q. Liu, Y. Ma, S.-P. Yan, P. Cheng, D.-Z. Liao, Cyano-bridged terbium(III)–chromium(III) bimetallic quasi-one-dimensional assembly exhibiting long-range magnetic ordering, Dalt. Trans. 41 (2012) 1624–1629. doi:10.1039/C1DT11655J.

[47] S. Chorazy, B. Sieklucka, S. Ohkoshi, Near-Infrared Photoluminescence in Hexacyanido-Bridged Nd–Cr Layered Ferromagnet, Cryst. Growth Des. 16 (2016) 4918–4925. doi:10.1021/acs.cgd.6b00476.

[48] H.L.C. Feltham, S. Brooker, Review of purely 4f and mixed-metal nd-4f single-molecule magnets containing only one lanthanide ion, Coord. Chem. Rev. 276 (2014) 1–33. doi:10.1016/j.ccr.2014.05.011.

[49] K.S. Pedersen, D.N. Woodruff, J. Bendix, R. Clérac, Experimental Aspects of Lanthanide Single-Molecule Magnet Physics, in: Lanthanides Actinides Mol. Magn., Wiley-VCH Verlag GmbH & Co. KGaA, Weinheim, Germany, 2015: pp. 125–152. doi:10.1002/9783527673476.ch5.

[50] K. Bernot, L. Bogani, A. Caneschi, D. Gatteschi, R. Sessoli, A Family of Rare-Earth-

Based Single Chain Magnets: Playing with Anisotropy, J. Am. Chem. Soc. 128 (2006) 7947–7956. doi:10.1021/ja061101l.

[51] O. Kahn, Chemistry and Physics of Supramolecular Magnetic Materials, Acc. Chem. Res. 33 (2000) 647–657. doi:10.1021/ar9703138.

[52] O. Guillou, P. Bergerat, O. Kahn, E. Bakalbassis, K. Boubekeur, P. Batail, M. Guillot, Ferromagnetically coupled gadolinium(III)copper(II) molecular material, Inorg. Chem. 31 (1992) 110–114. doi:10.1021/ic00027a021.

[53] M.L. Kahn, P. Lecante, M. Verelst, C. Mathonière, O. Kahn, Structural Studies and Magnetic Properties of Polymeric Ladder-Type Compounds {Ln 2 [Ni(opba)] 3 }·S (Ln = Lanthanide Element; opba = o -Phenylenebis(oxamato), S = Solvent Molecules), Chem. Mater. 12 (2000) 3073–3079. doi:10.1021/cm001042p.

[54] M.L. Kahn, C. Mathonière, O. Kahn, Nature of the Interaction between Ln III and Cu II Ions in the Ladder-Type Compounds {Ln 2 [Cu(opba)] 3 }·S (Ln = Lanthanide Element; opba = ortho -Phenylenebis(oxamato), S = Solvent Molecules), Inorg. Chem. 38 (1999) 3692–3697. doi:10.1021/ic9811998.

[55] M. Evangelisti, F. Bartolomé, J. Bartolomé, M.L. Kahn, O. Kahn, Specific heat and magnetic interactions in spin ladder gadolinium and copper-based molecular ferromagnets, J. Magn. Magn. Mater. 196–197 (1999) 584–585. doi:10.1016/S0304-8853(98)00846-4.

[56] E. Pardo, R. Ruiz-García, J. Cano, X. Ottenwaelder, R. Lescouëzec, Y. Journaux, F. Lloret, M. Julve, Ligand design for multidimensional magnetic materials: a metallosupramolecular perspective, Dalt. Trans. (2008) 2780. doi:10.1039/b801222a.

[57] J. Ferrando-Soria, E. Pardo, R. Ruiz-García, J. Cano, F. Lloret, M. Julve, Y. Journaux, J. Pasán, C. Ruiz-Pérez, Synthesis, crystal structures and magnetic properties of M(II)Cu(II) chains (M = Mn and Co) with sterically hindered alkyl-substituted phenyloxamate bridging ligands., Chem. Eur. J. 17 (2011) 2176–88. doi:10.1002/chem.201002110.

[58] J. Ferrando-Soria, M.T.M. Rood, M. Julve, F. Lloret, Y. Journaux, J. Pasán, C. Ruiz-Pérez, O. Fabelo, E. Pardo, Influence of the alkaline earth cations on the topology of MII/CuII mixed-metal–organic frameworks (M = Ca, Sr and Ba), CrystEngComm. 14 (2012) 761. doi:10.1039/c1ce06203d.

[59] P.-S. Kuhn, L. Cremer, A. Gavriluta, K.K. Jovanović, L. Filipović, A.A. Hummer, G.E. Büchel, B.P. Dojčinović, S.M. Meier, A. Rompel, S. Radulović, J.B. Tommasino, D. Luneau, V.B. Arion, Heteropentanuclear Oxalato-Bridged nd-4f (n =4, 5) Metal Complexes with NO Ligand: Synthesis, Crystal Structures, Aqueous Stability and Antiproliferative Activity, Chem. Eur. J. 21 (2015) 13703–13713. doi:10.1002/chem.201502026.

[60] A. Gavriluta, N. Claiser, P.-S. Kuhn, G. Novitchi, J.B. Tommasino, O. Iasco, V. Druta, V.B. Arion, D. Luneau, Osmium-Nitrosyl Oxalato-Bridged Lanthanide-Centered Pentanuclear Complexes - Synthesis, Crystal Structures and Magnetic Properties, Eur. J. Inorg. Chem. 2015 (2015) 1616–1624. doi:10.1002/ejic.201500023.

[61] F.R.F.R. Fortea-Pérez, J. Vallejo, M. Julve, F. Lloret, G. De Munno, D. Armentano, E. Pardo, Slow magnetic relaxation in a hydrogen-bonded 2D array of mononuclear dysprosium(III) oxamates., Inorg. Chem. 52 (2013) 4777–4779. doi:10.1021/ic4005517.

[62] G. Calvez, K. Bernot, O. Guillou, C. Daiguebonne, A. Caneschi, N. Mahé, Sterically-

induced synthesis of 3d–4f one-dimensional compounds: A new route towards 3d–4f single chain magnets, Inorganica Chim. Acta. 361 (2008) 3997–4003. doi:10.1016/j.ica.2008.03.040.

[63] M. Andruh, I. Ramade, E. Codjovi, O. Guillou, O. Kahn, J.C. Trombe, Crystal structure and magnetic properties of [Ln2Cu4] hexanuclear clusters (where Ln = trivalent lanthanide). Mechanism of the gadolinium(III)-copper(II) magnetic interaction, J. Am. Chem. Soc. 115 (1993) 1822–1829. doi:10.1021/ja00058a029.

[64] J. Paulovič, F. Cimpoesu, M. Ferbinteanu, K. Hirao, Mechanism of Ferromagnetic Coupling in Copper(II)-Gadolinium(III) Complexes, J. Am. Chem. Soc. 126 (2004) 3321–3331. doi:10.1021/ja030628k.

[65] E. Cremades, S. Gómez-Coca, D. Aravena, S. Alvarez, E. Ruiz, Theoretical Study of Exchange Coupling in 3d-Gd Complexes: Large Magnetocaloric Effect Systems, J. Am. Chem. Soc. 134 (2012) 10532–10542. doi:10.1021/ja302851n.

[66] J.-L. Liu, Y.-C. Chen, M.-L. Tong, Symmetry strategies for high performance lanthanide-based single-molecule magnets, Chem. Soc. Rev. 47 (2018) 2431–2453. doi:10.1039/C7CS00266A.

[67] S.K. Gupta, R. Murugavel, Enriching lanthanide single-ion magnetism through symmetry and axiality, Chem. Commun. 54 (2018) 3685–3696. doi:10.1039/C7CC09956H.

[68] L. Ungur, W. Van den Heuvel, L.F. Chibotaru, Ab initio investigation of the non-collinear magnetic structure and the lowest magnetic excitations in dysprosium triangles, New J. Chem. 33 (2009) 1224. doi:10.1039/b903126j.

[69] J.M. Kosterlitz, D.J. Thouless, Ordering, metastability and phase transitions in two-dimensional systems, J. Phys. C Solid State Phys. 6 (1973) 1181–1203. doi:10.1088/0022-3719/6/7/010.

[70] SAINT, version 6.45; Bruker Analytical X-ray Systems; Madison, WI, (2003).

[71] W. Sheldrick G.M. SADABS Program for Absorption Correction, version 2.10, Analytical X-ray Systems, Madison, SADABS Program for Absorption Correction, version 2.10, Analytical X-ray Systems, Madison, WI, (2003).

[72] Q. Li, W. Zhang, O.S. Miljanić, C.B. Knobler, J.F. Stoddart, O.M. Yaghi, A metal-organic framework replete with ordered donor-acceptor catenanes., Chem. Commun. 46 (2010) 380–382. doi:10.1039/b919923c.

[73] H. Furukawa, N. Ko, Y.B. Go, N. Aratani, S.B. Choi, E. Choi, A.O. Yazaydin, R.Q. Snurr, M. O'Keeffe, J. Kim, O.M. Yaghi, Ultrahigh porosity in metal-organic frameworks., Science. 329 (2010) 424–428. doi:10.1126/science.1192160.

[74] R.A. Smaldone, R.S. Forgan, H. Furukawa, J.J. Gassensmith, A.M.Z. Slawin, O.M. Yaghi, J.F. Stoddart, Metalorganic frameworks from edible natural products, Angew. Chem. Int. Ed. 49 (2010) 8630–8634. doi:10.1002/anie.201002343.

[75] A. Coskun, M. Hmadeh, G. Barin, F. Gándara, Q. Li, E. Choi, N.L. Strutt, D.B. Cordes, A.M.Z. Slawin, J.F. Stoddart, J.P. Sauvage, O.M. Yaghi, Metal-organic frameworks incorporating copper-complexed rotaxanes, Angew. Chem. Int. Ed. 51 (2012) 2160–2163. doi:10.1002/anie.201107873.

[76] G.M. Sheldrick, A short history of SHELX., Acta Crystallogr. A. 64 (2008) 112–122. doi:10.1107/S0108767307043930.

[77] W.S.-2013/4 B.A.X.I. Madison, SHELXTL-2013/4, Bruker Analytical X-ray

Instruments, Madison, WI, (2013).

[78] A.L. Spek, Structure validation in chemical crystallography, Acta Crystallogr. Sect. D Biol. Crystallogr. 65 (2009) 148–155. doi:10.1107/S090744490804362X.

[79] C. Palmer, D. CRYSTAL MAKER, Cambridge University Technical Services, CRYSTAL MAKER, Cambridge University Technical Services, Cambridge, (1996).

[80] L.J. Farrugia, WinGX suite for small-molecule single-crystal crystallography, J. Appl. Crystallogr. 32 (1999) 837–838. doi:10.1107/S0021889899006020.

[81] P.L.P.-R. version 3.6.2, Persistence of Vision Raytracer, POV-Ray, version 3.6.2; Persistence of Vision Raytracer, Pty. Ltd., (2003).

[82] F. Neese, The ORCA program system, Wires Comput Mol Sci. 2 (2012) 73–78. doi:10.1002/wcms.81.

[83] A. Schafer, C. Huber, R. Ahlrichs, Fully Optimized Contracted Gaussian-Basis Sets of Triple Zeta Valence Quality for Atoms Li to Kr, J. Chem. Phys. 100 (1994) 5829–5835. doi:10.1063/1.467146.

[84] K. Eichkorn, O. Treutler, H. Öhm, M. Häser, R. Ahlrichs, Auxiliary basis sets to approximate Coulomb potentials (Chem. Phys. Letters 240 (1995) 283-290), Chem. Phys. Lett. 242 (1995) 652–660. doi:10.1016/0009-2614(95)00838-U.

[85] C. van Wüllen, Molecular density functional calculations in the regular relativistic approximation: Method, application to coinage metal diatomics, hydrides, fluorides and chlorides, and comparison with first-order relativistic calculations, J. Chem. Phys. 109 (1998) 392–399. doi:10.1063/1.476576.

[86] D.A. Pantazis, X.-Y. Chen, C.R. Landis, F. Neese, All-Electron Scalar Relativistic Basis Sets for Third-Row Transition Metal Atoms, J. Chem. Theory Comput. 4 (2008) 908–919. doi:10.1021/ct800047t.

[87] M. Bühl, C. Reimann, D.A. Pantazis, T. Bredow, F. Neese, Geometries of Third-Row Transition-Metal Complexes from Density-Functional Theory, J. Chem. Theory Comput. 4 (2008) 1449–1459. doi:10.1021/ct800172j.

[88] D.A. Pantazis, F. Neese, All-Electron Scalar Relativistic Basis Sets for the Lanthanides, J. Chem. Theory Comput. 5 (2009) 2229–2238. doi:10.1021/ct900090f.

[89] D.A. Pantazis, F. Neese, All-Electron Scalar Relativistic Basis Sets for the Actinides, J. Chem. Theory Comput. 7 (2011) 677–684. doi:10.1021/ct100736b.

[90] D.A. Pantazis, F. Neese, All-electron scalar relativistic basis sets for the 6p elements, Theor. Chem. Acc. 131 (2012) 1292. doi:10.1007/s00214-012-1292-x.

FIGURES

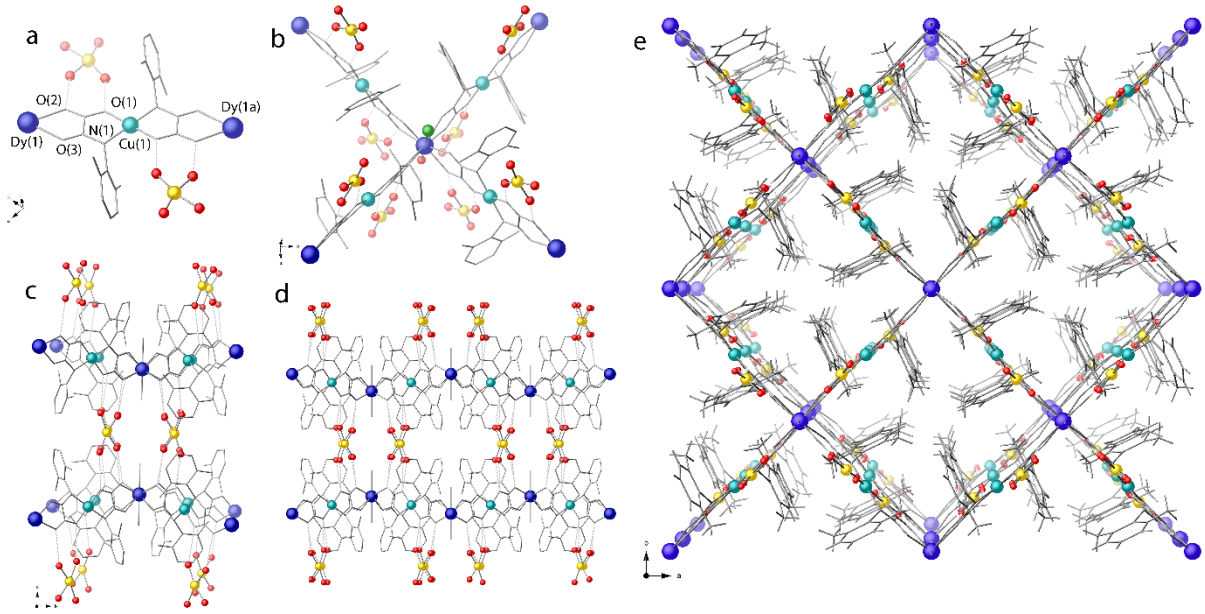

Fig. 1. View of fragments of the anionic network of **1**. $[Cu^{II}(Me_2pma)]^{2-}$ entities acting as bridge toward Dy^{III} metal ions together with $Li(H_2O)_4^+$ countercations H-bounded to oxamate moieties (a,b). Views along *a* and *c* directions of $\{Dy^{III}[Cu(Me_2pma)_2]_2Cl(H_2O)\}^{2-}$ square-grids interconnected by $Li(H_2O)_4^+$ ions (c-e). Cu, Dy, Li and O atoms are depicted as green, blue, gold and red spheres, respectively, whereas ligands are represented by sticks.

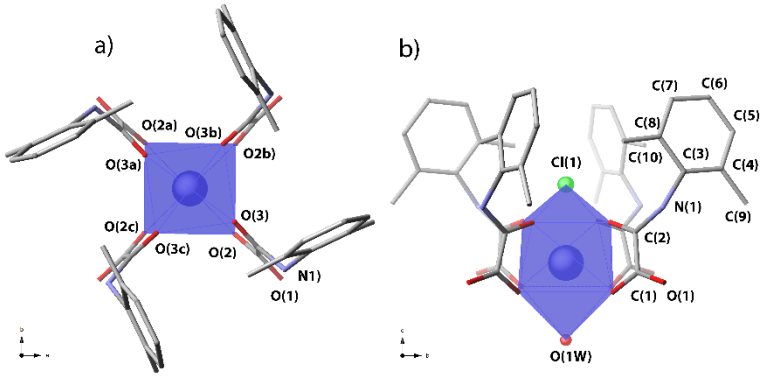

Fig. 2. Views of the Dy^{III} coordination polyhedron of **1** showing the bicapped cubic geometry with the labelling of the metal coordination environment in the *ab* (a) and *bc* (b) planes, respectively. Dysprosium, water-oxygen and chlorine atoms are represented by blue, red and green spheres, respectively, whereas ligands are represented by sticks.

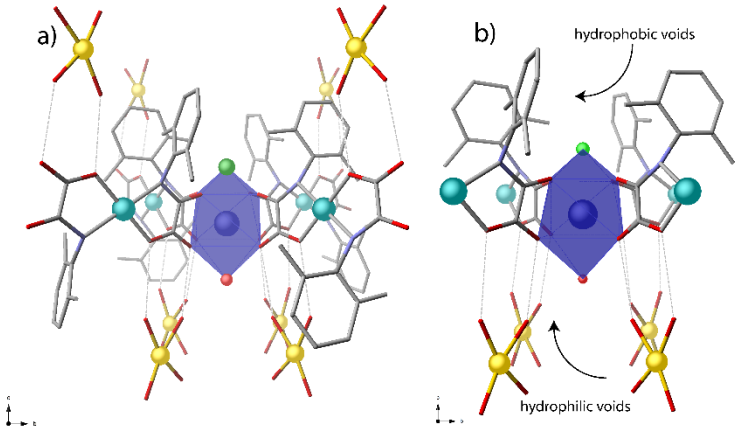

Fig. 3. Perspective views of the $\{Dy^{III}[Cu(Me_2pma)_2]_2Cl(H_2O)\}^{2-}$ entities and tetraaqua species $Li(H_2O)_4^+$ in the *bc* (b) planes, with details of dimethyl-substituted phenylene ligands orientation and resulting voids. Dysprosium, coordinated water-oxygen and chlorine atoms are represented by blue, red and green spheres, respectively, whereas ligands and Li^+ water environment are represented by sticks.

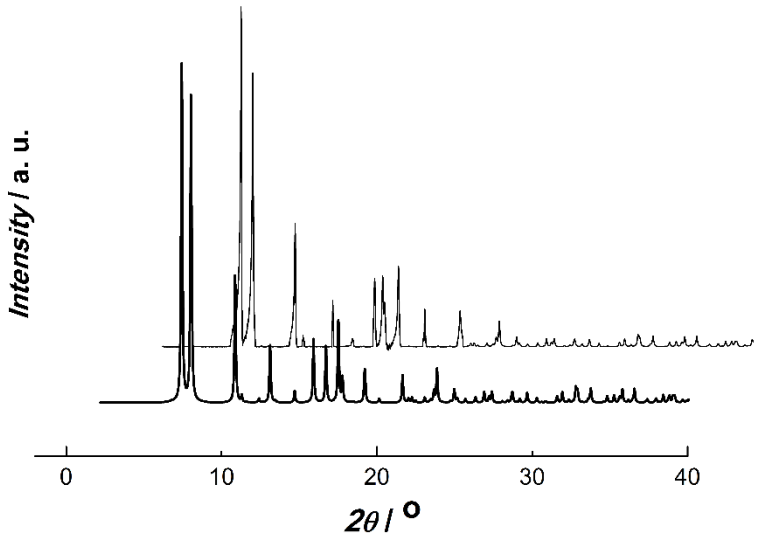

Fig. 4. Calculated (bold line) and experimental (normal line) PXRD pattern profiles of **1**.

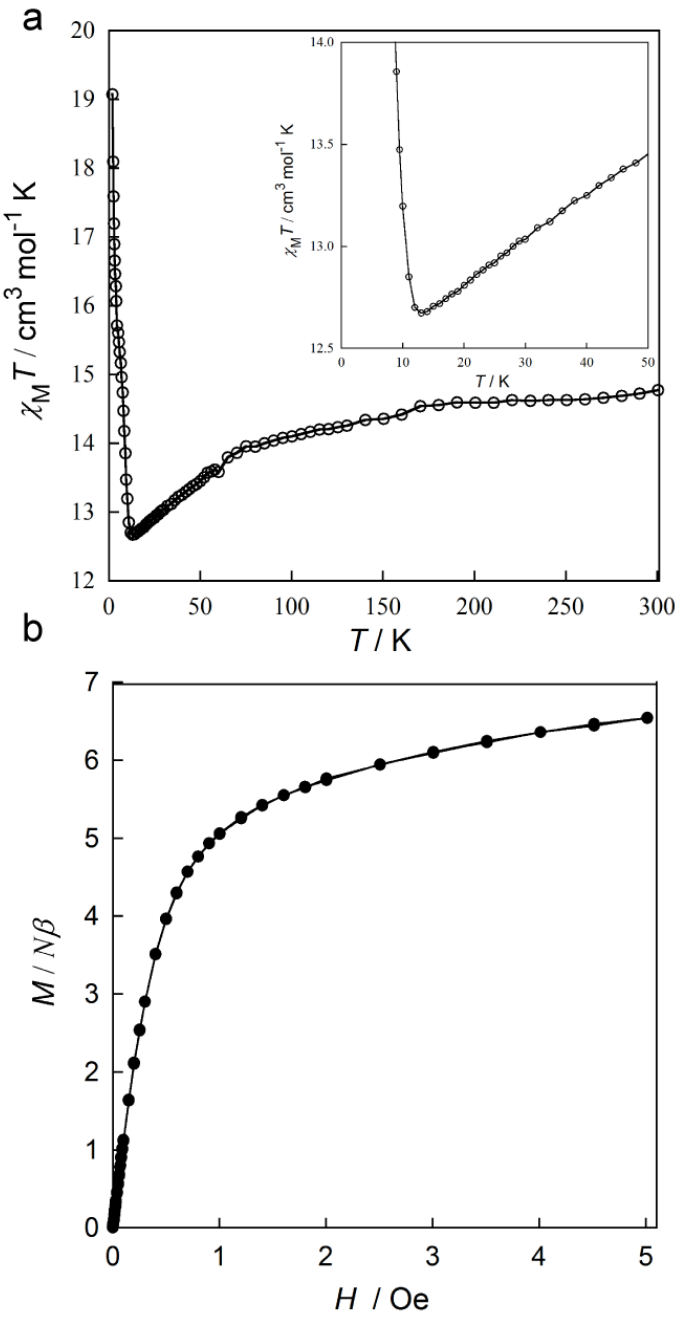

Fig. 5. (a) Temperature dependence of $\chi_M T$ for **1** under an applied dc field of 100 Oe (T < 50 K) and 1 T ($T \geq$ 50 K). The inset shows the minimum of $\chi_M T$ in detail. (b) Field dependence of M at 2.0 K.

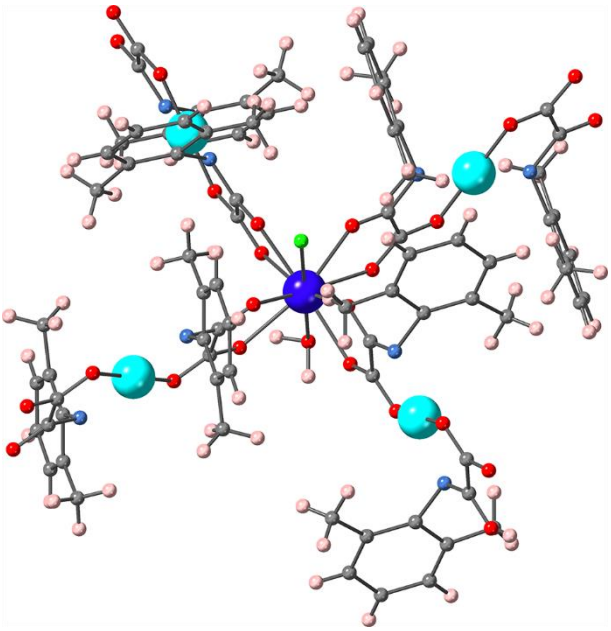

Fig. 6. View of the $DyZn_4$ molecular model used in CASSCF and CASSCF/NEVPT2 calculations and built from the experimental geometry of **1**. For clarity, the hydrogen atoms are masked.

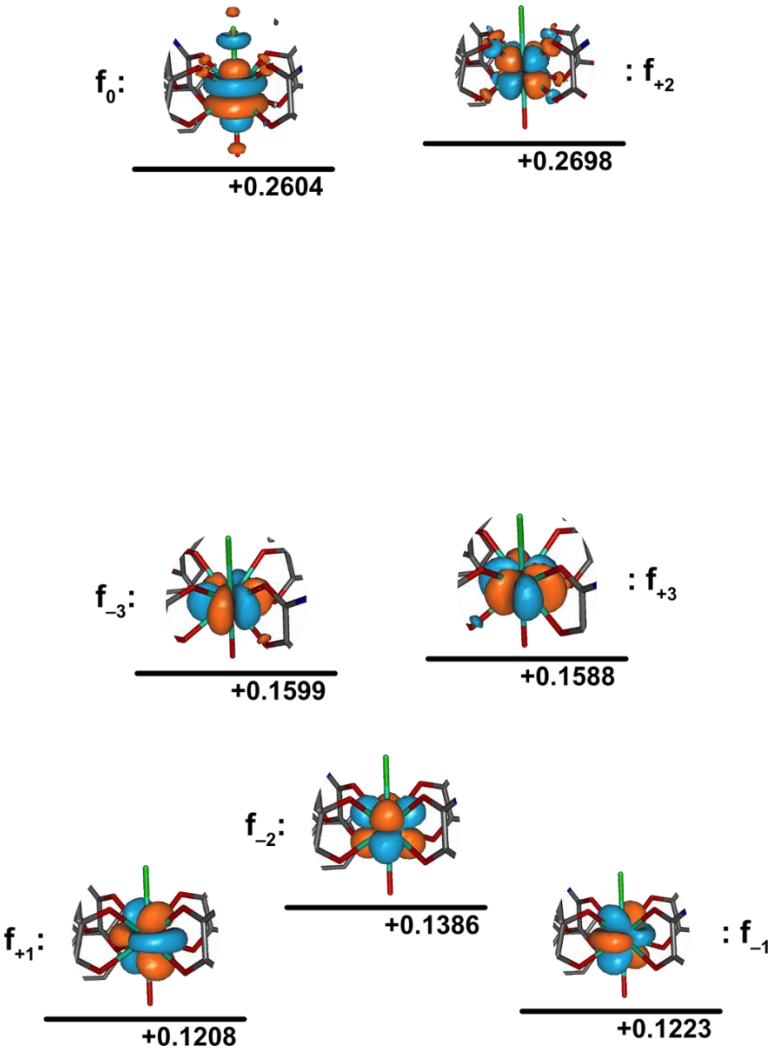

Fig. 7. Splitting of the f orbitals by the crystal field obtained from a CASSCF calculation on a $DyZn_4$ model built from the experimental geometry of **1**. The isodensity surfaces of natural orbitals correspond to a cut-off value of 0.01 e $bohr^{-3}$. The labels states the correspondence with the pure f orbitals. The values corresponds to the energies in eV for the natural orbitals of which the contribution of f orbitals prevails. For clarity only a cut on the molecular core composed of the Dy^{III} ion and the coordination environment is visualized.

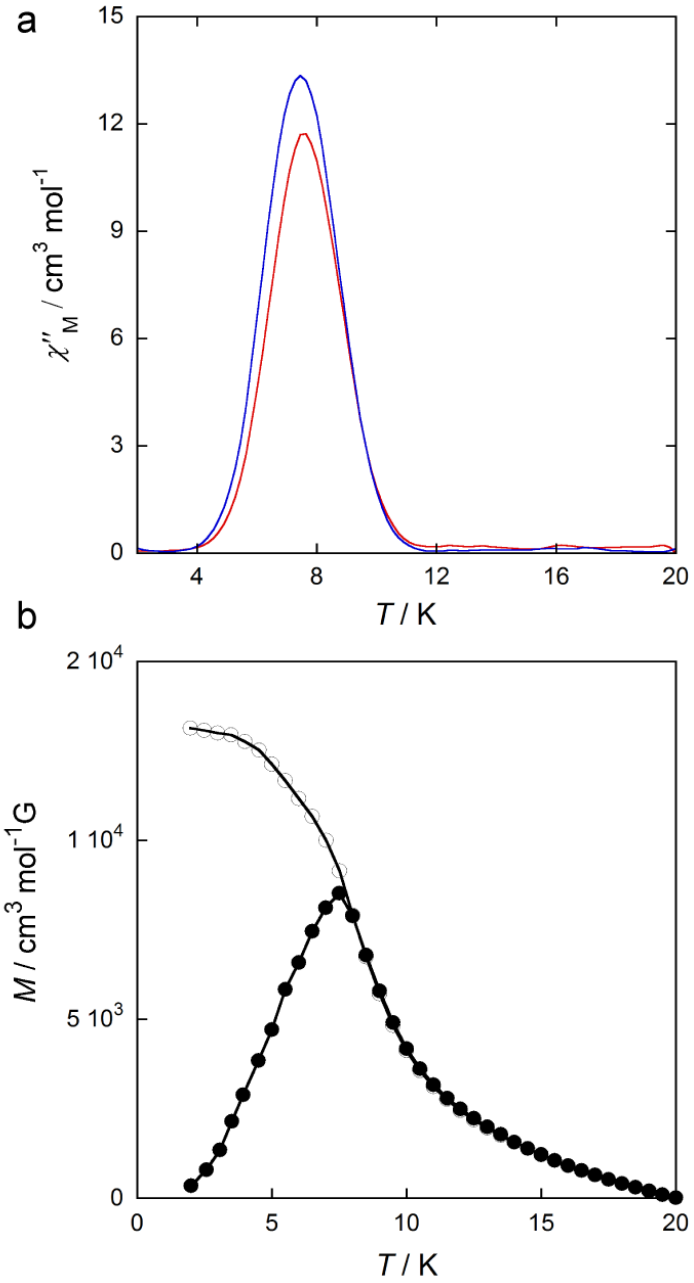

Fig. 8. (a) Temperature dependence of the out-of-phase *ac* magnetic susceptibility χ_M'' for **1** in an oscillating 1.0 Oe field at frequencies of 100 (red) and 1000 (blue) Hz. (b) FCM (•) (measured upon cooling within a field of 50 Oe) and ZFCM (○) (measured after cooling in zero field and then warming within the field) for **1**.

Supplementary Information (SI) for the manuscript:

Magnetic order in a Cu^{II}-Dy^{III} oxamato-based two-dimensional coordination polymer

Alejandro Pascual-Álvarez,[†] Joan Cano,[†] Francesc Lloret,[†] Jesús Ferrando-Soria,[†] Donatella Armentano[§] and Emilio Pardo*[†]*

Experimental Section

Preparation of $Li_2[Cu(Me_2pma)_2] \cdot 2H_2O$: A green polycrystalline solid was obtained from a metathesis from the previously reported tetrabutylammonium complex $(n\text{-}Bu_4N)_2[Cu(Me_2pma)_2] \cdot 2H_2O$ (4.8 g, 5 mmol), with $AgNO_3$ (1.70 g, 10 mmol) and (LiCl) (0.42 g, 10 mmol) in 25 mL of water. After eliminating AgCl by filtration, the solution was evaporated to dryness. The solid was collected and washed with a small amount of ethanol, acetone and diethyl ether and dried under vacuum. (2.31 g, 89 %). Elemental analysis calcd (%) for $C_{20}H_{22}N_2O_8Li_2Cu$ (495.8): C 48.45, H 4.47, N 5.65; found: C 48.32, H 4.21, N 5.66; IR (KBr): ν = 1653, 1621 cm^{-1} (C=O).

Theoretical calculations. The calculations were carried out with the version 4.0 of the ORCA programme,[1] using the TZVP basis set proposed by Ahlrichs[2] and the auxiliary TZV/C Coulomb fitting basis sets.[3] Relativistic effects were introduced from a zero-order regular approximation (ZORA).[4] Segmented all-electron relativistically contracted set for use with the ZORA Hamiltonian was employed for the dysprosium atom.[5] RIJCOSX method was used combining resolution of the identity (RI) and "chain of spheres" COSX approximations for the Coulomb and exchange terms, respectively.[6]

---

[1] F. Neese, *Wiley Interdiscip. Rev.: Comput. Mol. Sci*., 2012, **2**, 73

[2] (a) A. Schafer, H. Horn and R. Ahlrichs, *J. Chem. Phys*., 1992, **97**, 2571; (b) A. Schafer, C. Huber and R. Ahlrichs, *J. Chem. Phys.,* 1994, **100**, 5829

[3] (a) K. Eichkorn, O. Treutler, H. Ohm, M. Haser and R. Ahlrichs, *Chem. Phys. Lett*., 1995, **240**, 283; (b) K. Eichkorn, O. Treutler, H. Ohm, M. Haser and R. Ahlrichs, *Chem. Phys. Lett*., 1995, **242**, 652; (c) K. Eichkorn, F. Weigend, O. Treutler, H. Ohm and R. Ahlrichs, *Theor. Chem. Acc*., 1997, **97**, 19.

[4] C. Chang, M. Pelissier and Ph. Durand, *Phys. Scr.,* 1986, **34**, 394.

[5] (a) doi: 10.1021/ct800047t.; (b) **DOI:** 10.1021/ct800172j; (c) 10.1021/ct900090f;(d) 10.1021/ct100736b; (e) 10.1007/s00214-012-1292-x.

[6] (a) S. Kossmann and F. Neese, *J. Chem. Theory Comput*., 2010, **6**, 2325; (b) S. Kossmann and F. Neese, *Chem. Phys. Lett*., 2009, **481**, 240.

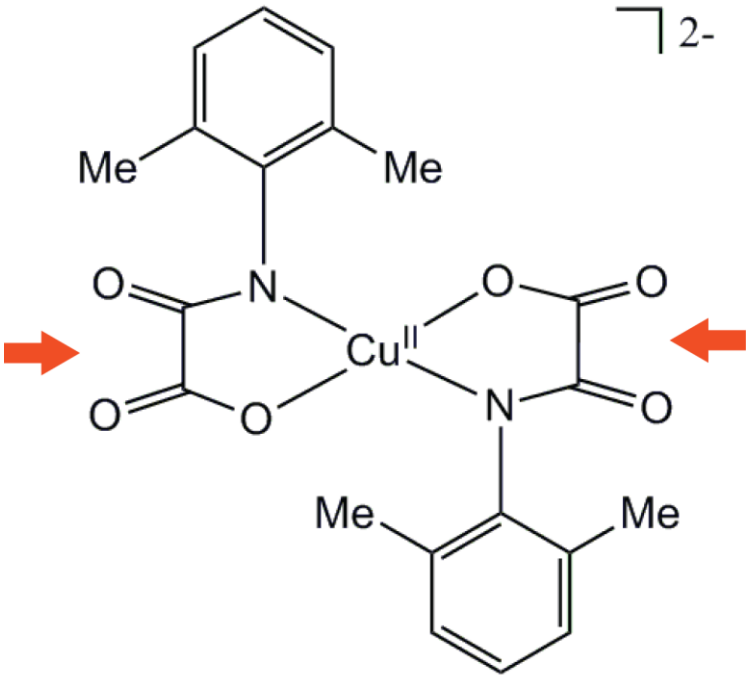

Scheme S1. Chemical structure of the mononuclear copper(II) anionic complex of formula $[Cu^{II}(Me_2pma)_2]^{2-}$, highlighting the free carbonyl groups acting as potential coordination sites (orange arrows).

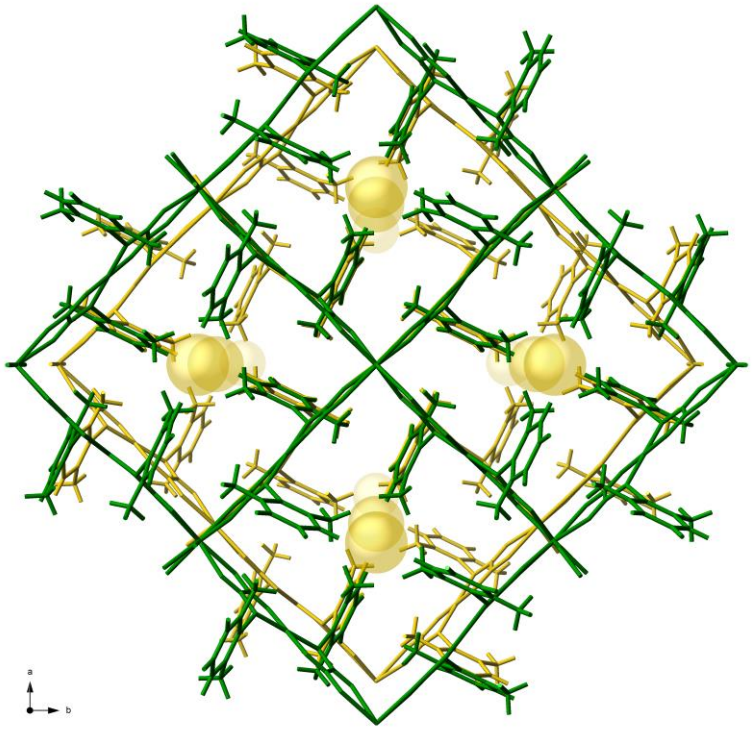

Figure S1. Crystal packing view of **1** along the *c* axis showing small hydrophobic voids. The coordination networks are represented with yellow and green sticks. The gold spheres represent the void space.

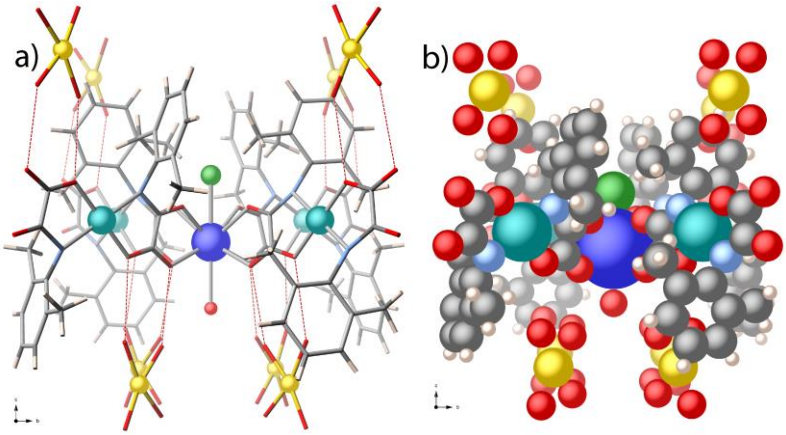

Figure S2. Perspective view, as balls and sticks and space filling model (a-b), of Dy(III) environment details in the $\{Dy^{III}[Cu(Me_2pma)_2]_2Cl(H_2O)\}^{2-}$ square-grids motif in **1**, interconnected by H-bonded $Li(H_2O)_4^+$ ions (red dashed lines) showing the basket-like cavity generated filled by water molecules and Chlorine atoms.

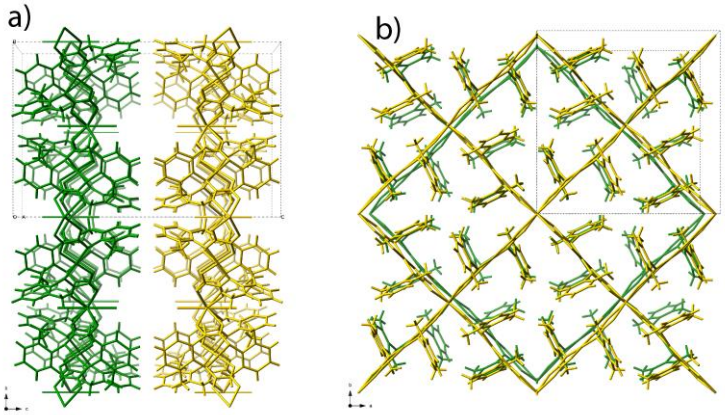

Figure S3. Perspective views of the eclipsed packing of the adjacent layers of **1** along the *c* (a) and *c* (b) axis, respectively. The two adjacent planes are depicted in yellow and green colors. The countercations and the solvent molecules have been omitted for clarity.

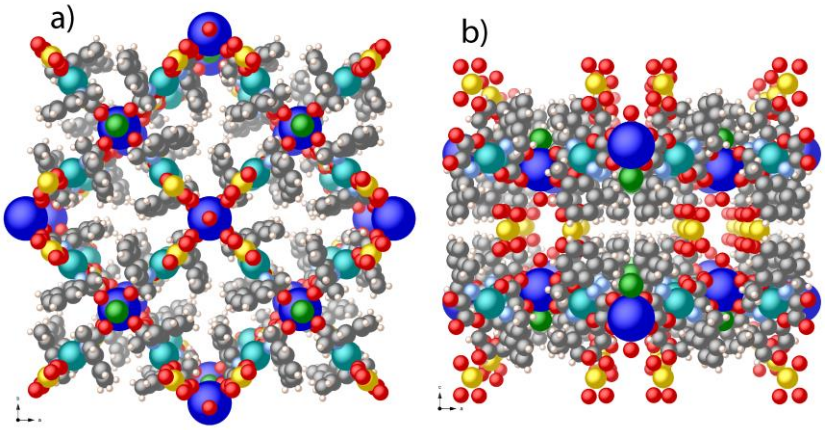

Figure S4. Space filling views along *c* and *b* directions of $\{Dy^{III}[Cu(Me_2pma)_2]_2Cl(H_2O)\}^{2-}$ square-grids interconnected by $Li(H_2O)_4^+$ ions (a-b). Cu, Dy, Li, O, N, C and H atoms are depicted as green, blue, gold, red, sky blue, gray and white spheres, respectively.

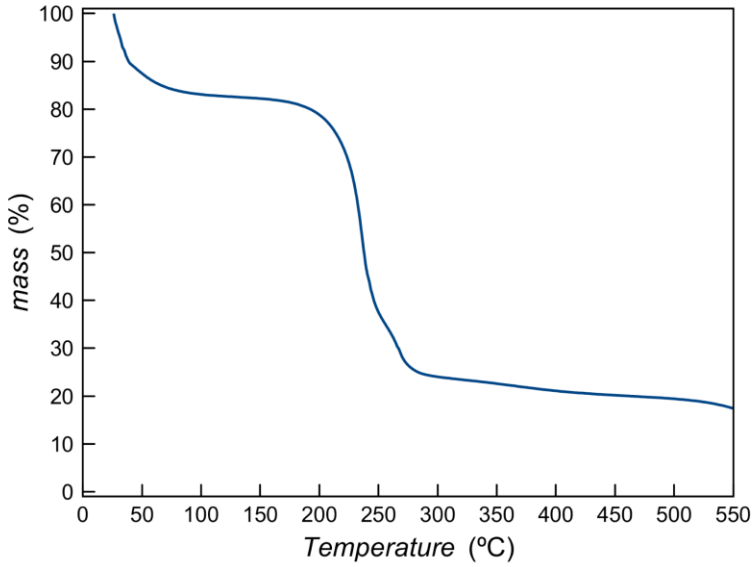

Figure S5. Thermogravimetric Analysis of **1** under dry N_2 atmosphere in the 25-550 ºC range.

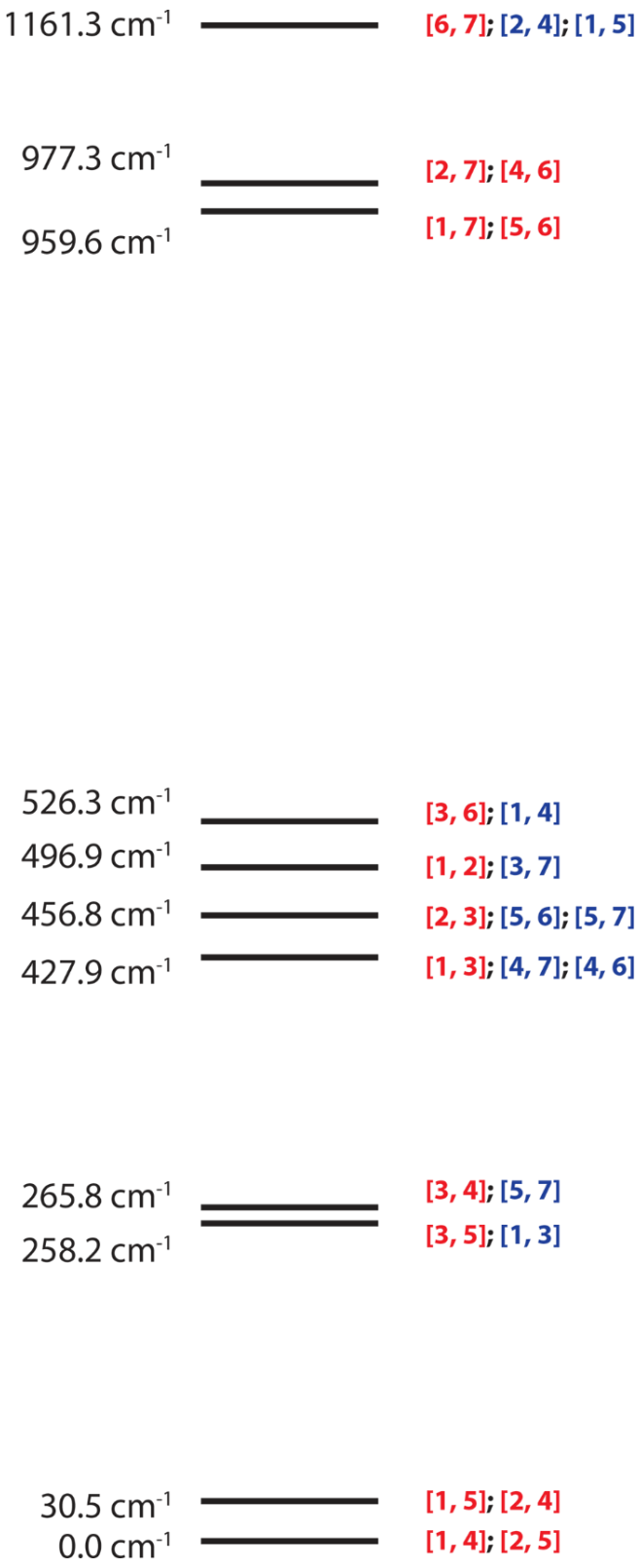

Fig. S6. Schematic energy diagram of the splitting of the ^{6}H term by crystal filed in **1**. Values correspond to the energies in cm^{-1}. Labels shows the electronic configurations that mainly contribute to a particular state. Red and blue colors are used for strong and moderate contributions. Each electronic configuration is noted indicating the electrons occupy an f orbital following the energetic order displayed in Fig. 7: {f_{-1}, f_{+1}, f_{-2}, f_{+3}, f_{-3}, f_{0}, f_{+2}}. In the shown electronic configurations, one electron is placed in each one of these f orbital and only a second electron is in *i* and *j* orbitals, being [*i*, *j*] a simplified notation of an electronic configuration. Thus, [1,3] refers to the {2,1,2,1,1,1,1} electronic configuration.